Diameter-dependent bending dynamics of single-walled carbon nanotubes in liquids

Nikta Fakhri[a,b], Dmitri A. Tsyboulski[c,d], Laurent Cognet[c,e], R. Bruce Weisman[c,d,f], and Matteo Pasquali[a,b,c,d,f,1]

Departments of [a]Chemical and Biomolecular Engineering and [c]Chemistry, [f]NanoCarbon Center, [b]Center for Biological and Environmental Nanotechnology, and [d]R. E. Smalley Institute for Nanoscale Science and Technology, Rice University, Houston, TX 77005; and [e]Centre de Physique Moléculaire Optique et Hertzienne, Université de Bordeaux, and Centre National de la Recherche Scientifique, Talence F-33405, France

Edited by Harry L. Swinney, University of Texas, Austin, TX, and approved June 30, 2009 (received for review April 15, 2009)

By relating nanotechnology to soft condensed matter, understanding the mechanics and dynamics of single-walled carbon nanotubes (SWCNTs) in fluids is crucial for both fundamental and applied science. Here, we study the Brownian bending dynamics of individual chirality-assigned SWCNTs in water by fluorescence microscopy. The bending stiffness scales as the cube of the nanotube diameter and the shape relaxation times agree with the semiflexible chain model. This suggests that SWCNTs may be the archetypal semiflexible filaments, highly suited to act as nanoprobes in complex fluids or biological systems.

actin | microrheology | semiflexible filaments and polymers | stochastic dynamics | nanomechanics

Single-walled carbon nanotubes (SWCNTs) are tubular nanostructures of covalently bonded carbon atoms, with typical diameters near 1 nm and lengths in the micrometer range. Their remarkable combination of very large aspect ratios, high mechanical strength, and versatile electronic properties makes SWCNTs highly suited for many applications, e.g., in material engineering, soft matter science, and biomedicine (1, 2). However, advances in applications are presently limited by scant fundamental understanding of their mechanical and dynamical behavior in fluid environments. When embedded in a viscous medium, the dynamics of these 1D nanoobjects are essentially dominated by the balance of Brownian forces, which tend to bend them, and elastic forces, which oppose this curvature. The simplest model for such filaments is that of an inextensible elastic beam with bending stiffness $\kappa = EI$, where E is the elastic modulus and I is the area moment of inertia about the filament axis. The ratio of bending stiffness to thermal energy yields a characteristic persistence length $L_p = \kappa/k_BT$, where k_B is the Boltzmann constant, and T is the absolute temperature (3). This is the length scale over which the filament shows significant curvature induced by thermal fluctuations. Hence, "short" filaments ($L \ll L_p$) essentially appear as rigid rods, whereas "long" filaments ($L \gg L_p$) display significant bending.

SWCNT persistence length is important in a variety of applications such as organization on patterned surfaces (4), the ability to form liquid crystals (5), and the stiffening of polymeric networks (6, 7). Although various methods have been used to infer or measure these persistence lengths, there is still controversy about whether, in the absence of flow, individual SWCNTs in liquids should be considered rigid ($L \ll L_p$) or semiflexible ($L \approx L_p$). A study based on the size of closed SWCNT rings estimated a persistence length of 800 nm (8); experimental data from neutron scattering indicated that SWCNTs behave as rigid rods on length scales of at least ≈150 nm (9), and X-ray scattering data suggested that SWCNTs do not display rod-like behavior at any length (10). Fluorescence video microscopy studies of fluorescently labeled SWCNTs deduced persistence lengths ranging between 32 and 174 μm (11), although this method could not distinguish between individual SWCNTs and small bundles. Theory based on a continuum model for a hollow cylinder of radius R predicts (12–14) the bending stiffness of SWCNTs to be $\kappa = \pi CR^3$, where the "in-plane stiffness" C is estimated as ≈345 J/m^2 from ab initio calculations of the elastic energy of a tube under axial strain (12). This model suggests that bending stiffness, and hence persistence length, should depend strongly on nanotube diameter. To date, however, no experimental test of such a relationship has been reported.

Fluorescence microscopy is a powerful tool for studying the mechanical properties of one-dimensional nanoobjects by directly measuring their individual shape fluctuations. Variants of this technique have been used to measure the bending stiffness of biopolymers such as actin and microtubules (15–18). Here, we exploit the intrinsic near-infrared fluorescence of semiconducting SWCNTs to image individual nanotubes moving freely in aqueous surfactant suspension as they undergo Brownian motion in a quasi-two-dimensional sample chamber (19, 20). The use of intrinsic fluorescence provides three benefits. First, because nanotubes are imaged by using their own characteristic emission rather than that of an added fluorophore, all observed objects are confidently identified as SWCNTs. Second, aggregation of SWCNTs into bundles strongly quenches the emission, so there is good discrimination against nanotube bundles. Finally, the wavelength of a nanotube's near-infrared fluorescence is characteristic of its exact transverse structure (21), so spectral analysis reveals individual SWCNT diameters. Fig. 1 shows the thermally induced undulations of a SWCNT visualized by this technique. The bending rigidity (persistence length) of each individual SWCNT can be determined from the amplitude of such shape fluctuations (16, 22).

We analyzed 34 individual nanotubes with diameters between 0.7 and 1.2 nm. Measurements were restricted to those with lengths >3 μm to minimize systematic errors in nanotube shape determinations due to pixilation and diffraction. Moreover, we used only SWCNTs that showed identical emission spectra along their lengths, indicating an absence of major structural defects (e.g., chirality switch) or bundling with another nanotube (20). In a typical experiment, 1,000 images of each SWCNT were acquired. The backbone coordinates of the SWCNTs were determined with subpixel accuracy by an intensity-weighted analysis (see *Methods* below and Fig. 2*A*). Treating SWCNTs as worm-like chains (22) and following the procedure of Gittes et al. (16), the shape of the SWCNT in each image was expressed as a sum of cosine bending modes (which form an orthogonal basis); mode amplitudes were computed by projecting the image shape onto these basis functions.

Fig. 2*B* shows the results compiled from applying this procedure to all 1,000 images in a sequence recorded for one

Author contributions: N.F., D.A.T., L.C., R.B.W., and M.P. designed research; N.F., D.A.T., and L.C. performed research; N.F., D.A.T., and L.C. analyzed data; and N.F., D.A.T., L.C., R.B.W., and M.P. wrote the paper.

The authors declare no conflict of interest.

This article is a PNAS Direct Submission.

[1]To whom correspondence should be addressed. E-mail: mp@rice.edu.

This article contains supporting information online at www.pnas.org/cgi/content/full/0904148106/DCSupplemental.

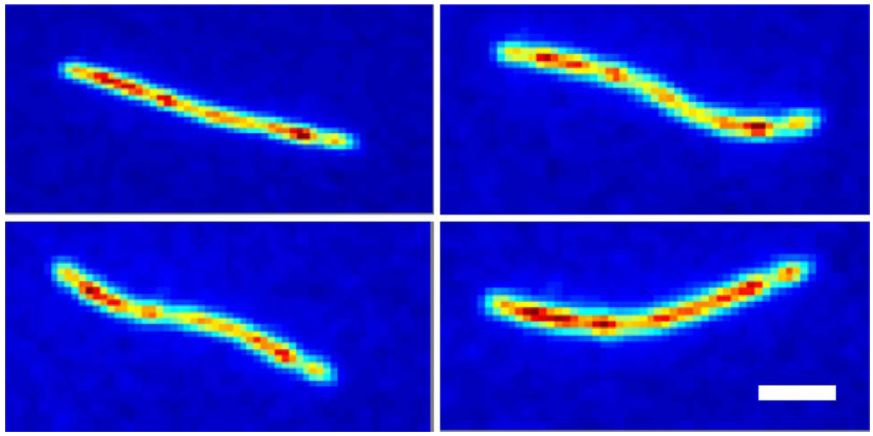

Fig. 1. Bending deformations of a nanotube. Representative near-infrared (false colored) fluorescence images of the same SWCNT in liquid suspension illustrating Brownian bending deformations. (Scale bar, 2 μm.) (See Movie S1 for typical examples of SWCNT bending dynamics.)

nanotube. Here, the variance in the amplitude of each bending mode is plotted vs. the mode number. The measured mean amplitude is essentially zero, confirming that this SWCNT had no static curvature. The longer wavelength (low n) modes show the expected n^{-2} dependence of amplitude on mode number, indicating that the measured variance is due to thermal fluctuations. This n^{-2} dependence breaks down for higher modes (typically $n > 5$) because systematic errors due to image pixilation and diffraction effects start to dominate those mode amplitudes (16). The analysis of mode amplitudes also provides an internal consistency test. For example, a structural defect in a nanotube should yield a locally lower stiffness, which would increase the amplitudes of specific modes and break the n^{-2} decay law. The fact that we observe no anomalies in the plots of amplitude variance vs. mode number suggests an absence of significant mechanical defects in the studied nanotubes.

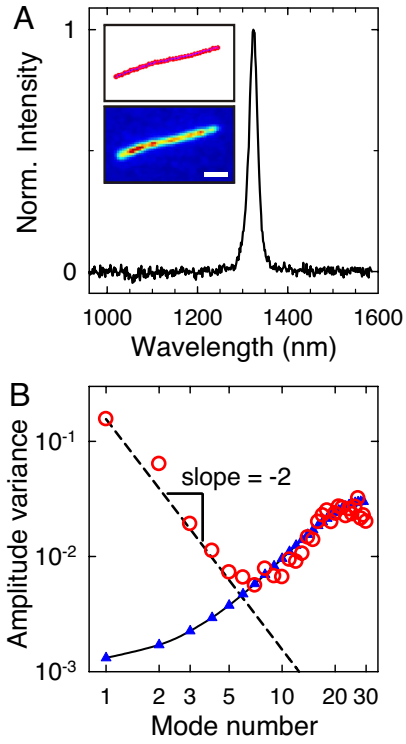

Fig. 2. Optical and mechanical spectra of an individual SWCNT undergoing Brownian motion. (*A*) Individual SWCNT emission spectrum with peak at 1,323 nm, implying a (9,7) structure, with a diameter of 1.09 nm. (*Inset*) Fluorescence image of the nanotube and corresponding filament coordinates. (*B*) Variance (in μm) of the amplitude of the bending modes for the (9,7) nanotube, plotted vs. mode number. Red circles are experimental data, and the dashed line represents the expected n^{-2} dependence. Beyond $n = 5$, the measured mode amplitudes are dominated by experimental noise. The estimated variance contributed by experimental noise is shown by blue triangles and the continuous black line (15, 16).

Fig. 3*A* shows how SWCNT persistence length (or bending stiffness) depends on SWCNT diameter. The experimental values of L_p range from 26 to 138 μm. We find that the measured bending stiffness scales with the cube of nanotube diameter, as predicted by the elastic continuum model (12). However, the bending stiffness relation $\kappa = \pi CR^3$ implies a value for in-plane stiffness C of 678 $\pm$ 22 J/m^2. This is approximately a factor of two larger than the value predicted theoretically (12). According to Odijk–Skolnick–Fixman theory (23, 24), the discrepancy cannot be explained by a stiffening effect from the ionic surfactant that coats the nanotube because the Debye length is only 1.7 nm under our experimental conditions. Moreover, the persistence length normalized by the nanotube diameter cubed shows no significant correlation with nanotube length (correlation coefficient of 0.022), as one would expect in such systems (Fig. 3*B*). There is also no apparent correlation between persistence length and SWCNT chiral angle (see Fig. S1).

Fourier modes provide a convenient basis for describing dynamic as well as static SWCNT shapes. The relaxation times of the SWCNT deformations can be extracted from the exponential decay of the autocorrelation of Fourier mode amplitudes (see *Methods*). However, in this analysis, exposure times that are long relative to the relaxation time can blur images and depress the apparent shape fluctuations, thereby hampering the interpretation of nanotube dynamics. To minimize this source of error, we slowed the nanotube dynamics by raising the solvent viscosity with a mixture of sucrose and glucose. Fig. 4*A* shows experimental autocorrelation functions for the first and second bending modes. There is good consistency for data acquired with different exposure times, indicating that the image acquisition rate was adequate to capture undistorted dynamics. Brangwynne et al. (15) have shown that, although the cosines are not exactly normal modes, the relaxation of the first two modes is well approximated by a single exponential. The data in Fig. 4*A* are well fit by an exponential decay model, which gives the results shown as solid curves and provides the relaxation times τ_1 and τ_2 (for the first and second modes, respectively). Because all other relevant parameters (fluid viscosity, temperature, and SWCNT length) are known independently, the persistence length of each

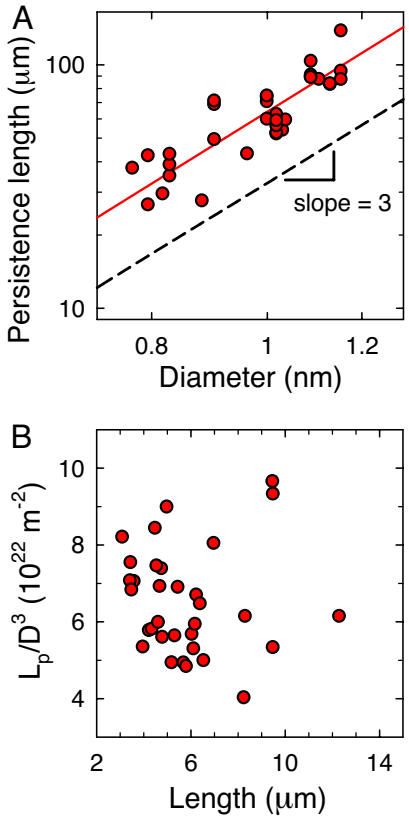

Fig. 3. Diameter dependence of persistence length. (*A*) Persistence length of 34 SWCNTs plotted as a function of their diameters. The black dotted line shows the prediction of the theoretical thin shell model, $\kappa = \pi CR^3$, using the ab initio calculated value of $C = 345$ J/m^2. The red line shows the experimental best fit (slope = 3 ± 0.37, $C = 678 \pm 22$ J/m^2). (*B*) Persistence length of 34 SWCNTs normalized by the diameter cubed plotted vs. the length. The correlation coefficient in this plot is 0.022.

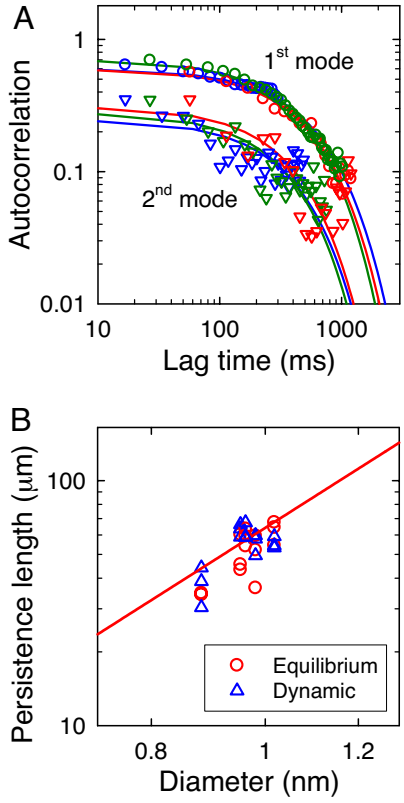

Fig. 4. SWCNT persistence lengths deduced from bending mode relaxation. (*A*) Shape autocorrelation data for the first bending mode (circles) and second bending mode (triangles) of a nanotube as calculated from image sequences with exposure times of 10, 20, and 50 ms (blue, green, and red, respectively). Solid lines of the same color show corresponding exponential decay best fits. The solution viscosity was increased by adding a sucrose/glucose mixture to slow the dynamics in this system. (*B*) Persistence length comparisons for five nanotubes as determined by using equilibrium bending analysis (red circles) and bending mode relaxation analysis (blue triangles) of the first bending mode for exposure times of 10, 20, and 50 ms. The red line shows the fit from Fig. 3*A*.

SWCNT can be extracted from the dynamic data by using the theoretical relationship between persistence length and bending relaxation times (25–28), $L_p \approx \gamma/\tau_n k_B T((n + \frac{1}{2})\pi/L)^4$, where $\gamma \approx 4\pi\eta/\ln(L/d)$ is the friction coefficient, and τ_n is the relaxation time of mode n (see *Methods*). Persistence length values extracted from the relaxation times of the first bending mode for five SWCNTs are in excellent agreement with our equilibrium bending analysis for the same nanotubes (see Fig. 4*B*). We consider such agreement remarkable, considering the simplified nature of the semiflexible chain model.

In summary, we have studied the Brownian bending dynamics of diameter-resolved SWCNTs in ordinary aqueous surfactant suspensions. The measured persistence lengths range from 26 to 138 μm for SWCNTs of diameter from 0.77 to 1.15 nm. Persistence length is found to scale with the cube of diameter, as expected from an elastic continuum model (12), but the deduced nanotube in-plane stiffness significantly exceeds a theoretically predicted value. Smaller values of persistence length reported in previous studies might reflect the presence of other forces in addition to Brownian ones, such as the intertube van der Waals attractions that control the structure of buckypaper. The persistence length of a SWCNT within our diameter range is comparable with that of actin filaments ($L_p \approx 17$ μm) but somewhat shorter than that of microtubules (L_p on the order of millimeters)—because the higher elastic modulus of the SWCNTs is counterbalanced by larger diameters of actin (≈7 nm) and microtubules (≈25 nm). Interestingly, based on the scaling of persistence length with CNT diameter, SWCNTs should be several orders of magnitude less stiff than their multiwalled counterparts (MWCNTs, diameter 10–50 nm) (13). The ultimate mesoscopic and macroscopic properties of functional materials such as fibers are dictated by the behavior of the constituent single molecules (13, 29). Understanding the relationship between single-molecule mechanics and the collective properties of their macromolecular assemblies has implications for the rational design of carbon nanotube-based functional materials (29, 30). We have shown that even small changes in diameter affect significantly the stiffness of SWCNTs. This result implies that larger diameter SWCNTs could yield stiffer fibers of low density—the density of SWCNTs scales inversely with their diameter. Interestingly, recent experimental results show that large-diameter single and double-walled carbon nanotubes yield fibers with the best mechanical properties achieved so far (30, 31)—although there are limitations, because excessively large few-walled carbon nanotubes are prone to buckle radially into flattened ribbons (32, 33). Because stiffness is an important property in biological systems, the diameter-dependent rigidity of SWCNTs should also be considered as a potentially important variable in studies of interactions of carbon nanotubes with cells.

When only Brownian forces are present, we observe that relatively short SWCNTs (below ≈3 μm) behave as rigid rods in ambient fluid suspension and show translational and rotational diffusion but essentially no shape fluctuations (11, 34). We find that the thermal shape fluctuations of longer SWCNTs accu-

rately follow the semiflexible filament model. Therefore, existing models for semiflexible networks should be applicable to the viscoelastic properties of concentrated SWCNT suspensions (35), possibly by constructing model networks with tunable stiffness by using diameter-sorted SWCNT samples (36). In addition, the varying persistence lengths within the family of SWCNT structures could be exploited to develop rod-like nano- and microscale probes for microrheological studies of complex fluids and biological systems and to tailor nanotube mobility in confined environments (37) such as living cells and tissues.

Methods

SWCNTs with diameters between 0.7 and 1.2 nm were obtained from the Rice University HiPco reactor (batches 125.2, 161.1, and 162.5). Dilute aqueous suspensions of SWCNTs (1–10 ng/mL) in SDBS (sodium dodecylbenzenesulfonate, 1 wt %) were prepared by mild ultrasonication (7 W, 5–6 s) to minimize SWCNT breaking. Suspended SWCNTs were imaged in a quasi-two-dimensional chamber $\approx 1.0 \pm 0.5$-μm thick made by sandwiching ≈ 0.7 μL of sample (1.0 μL for samples with higher viscosity) between a microscope slide and coverslip. The sample was sealed with vacuum grease to prevent convective flow due to evaporation. Enough time was allowed between sealing of the sample and image acquisition to ensure the cessation of any convective flow induced during sample preparation. All experiments were performed at room temperature (23 °C).

Near-infrared fluorescence images of individual nanotubes were recorded under a Nikon TE-2000 inverted microscope using 150× magnification (Nikon Plan Apo oil-immersion 100×, 1.4 N.A. objective and 1.5× auxiliary magnification), equipped with a liquid nitrogen-cooled NIR InGaAs camera (OMA-V 2D; Roper) (19). The microscope was fiber-optically coupled via one of its output ports to the input slit of a J-Y C140 spectrograph with a cryogenically cooled 512-element InGaAs array (OMA-V; Roper) for measuring spatially resolved emission spectra. Samples were excited with focused diode laser beams at 658 and 785 nm. The excitation intensity at the target was adjusted between $\approx$0.1 and 10 kW/cm^2 to capture high-quality image sequences. We confirmed that at these irradiation levels the excitation laser had no noticeable effects on SWCNT dynamics. To slow down the SWCNT dynamics for bending-mode relaxation analysis, the sample viscosity was increased by adding 1 μL of SWCNT suspension to 10 μL of a 60:40 sucrose/glucose solution (40% total sugar by mass in 1 wt % SDBS) to yield a final viscosity of $\approx$13 mPas. SWCNT images were acquired with exposure times of 50 ms for shape analysis and 10, 20, or 50 ms for relaxation time analysis.

An image analysis algorithm was developed to track the fluctuating shape of SWCNTs with high accuracy. First, the position of the SWCNT was estimated by thresholding the image. The coordinates of the backbone of the SWCNT were determined with an intensity-weighted center-of-mass method. A two-dimensional fixed-area kernel moved along the contour of the nanotube in the original image in 1-pixel steps. By measuring the center of intensity for each position of the kernel, the real-space coordinates of that point on the backbone were extracted to obtain a full set of SWCNT backbone coordinates (x_i,y_i). Following the procedure developed by Gittes et al. (16), the shape (tangent angle) of the nanotube, $\theta(s_i) = \tan^{-1}(y_{i+1} - y_i)/(x_{i+1} - x_i)$, was calculated from the backbone coordinates and decomposed into Fourier modes:

$$\theta(s) = \sqrt{\frac{2}{L}} \sum_{n=0}^{\infty} a_n \cos\left(\frac{n\pi s}{L}\right),$$

where n is the mode number, a_n is the mode amplitude, and L is the SWCNT contour length. The amplitude of each mode was extracted by taking the Fourier inverse of this equation. In the absence of external forces, the equipartition theorem dictates that the variance in the amplitude of the bending modes is inversely proportional to the bending rigidity:

$$\langle (a_n(t))^2 \rangle = \frac{k_B T}{\kappa} \frac{L^2}{(n\pi)^2},$$

where the angular brackets denote an ensemble average, which is equivalent to the time average because the system is ergodic. The cosine modes are not exactly normal modes for the dynamics of semiflexible filaments with free ends (15, 28), yet their dynamics is well approximated by single-exponential relaxation (15), and the relaxation times can be extracted from the autocorrelation of mode amplitudes:

$$\langle a_n(t + \delta) \cdot a_n(t) \rangle = |a_n(t) \cdot a_n(t)| e^{-\delta/\tau_n}.$$

It can be shown that the mode relaxation times τ_n are given by (16) $\tau_n \approx \gamma/\kappa q^4$. Here, $q \approx (n + \frac{1}{2})\pi/L$ and the hydrodynamic friction coefficient γ for a rod of length L and diameter d confined in a gap comparable to L can be approximated as twice the bulk friction coefficient (38), $\gamma \approx 4\pi\eta/\ln(L/d)$, where η is the bulk viscosity.

ACKNOWLEDGMENTS. We thank Rajat Duggal, Boris Yakobson, Howard Schmidt, and Fred MacKintosh for useful discussions. This work was supported by National Science Foundation (NSF) Grants CTS-CAREER 0134389 and CHE-0809020, NSF Center for Biological and Environmental Nanotechnology Grants EEC-0118007 and EEC-0647452, Robert A. Welch Foundation Grants C-0807 and C-1668, Applied NanoFluorescence, LLC, Welch Foundation Postdoctoral Fellowship L-C-0004 (to D.A.T.), the Fullbright Foundation (L.C.) and Délégation Générale pour l'Armement Grant ERE060016 (to L.C.).

1. Polizu S, Savadogo O, Poulin P, Yahia L (2006) Applications of carbon nanotubes-based biomaterials in biomedical nanotechnology. *J Nanosci Nanotechnol* 6:1883–1904.
2. Baughman RH, Zakhidov AA, de Heer WA (2002) Carbon nanotubes—The route toward applications. *Science* 297:787–792.
3. Doi M, Edwards SF (1986) *The Theory of Polymer Dynamics* (Oxford Univ Press, Oxford).
4. Geblinger N, Ismach A, Joselevich E (2008) Self-organized nanotube serpentines. *Nat Nanotechnol* 3:195–200.
5. Davis VA, et al. (2004) Phase behavior and rheology of SWNTs in superacids. *Macromolecules* 37:154–160.
6. Ajayan PM, Tour JM (2007) Materials science—Nanotube composites. *Nature* 447:1066–1068.
7. Kumar S, et al. (2002) Synthesis, structure, and properties of PBO/SWNT composites. *Macromolecules* 35:9039–9043.
8. Sano M, Kamino A, Okamura J, Shinkai S (2001) Ring closure of carbon nanotubes. *Science* 293:1299–1301.
9. Zhou W, et al. (2004) Small angle neutron scattering from single-wall carbon nanotube suspensions: Evidence for isolated rigid rods and rod networks. *Chem Phys Lett* 384:185–189.
10. Schaefer DW, Zhao J, Brown JM, Anderson DP, Tomlin DW (2003) Morphology of dispersed carbon single-walled nanotubes. *Chem Phys Lett* 375:369–375.
11. Duggal R, Pasquali M (2006) Dynamics of individual single-walled carbon nanotubes in water by real-time visualization. *Phys Rev Lett* 96:246104.
12. Kudin KN, Scuseria GE, Yakobson BI (2001) C2F, BN, and C nanoshell elasticity from ab initio computations. *Phys Rev B* 64:235406.
13. Yakobson BI, Couchman LS (2006) Persistence length and nanomechanics of random bundles of nanotubes. *J Nanoparticle Res* 8:105–110.
14. Yakobson BI, Avouris P (2001) Mechanical properties of carbon nanotubes. Carbon nanotubes. *Top Appl Phys* 80:287–327.
15. Brangwynne CP, et al. (2007) Bending dynamics of fluctuating biopolymers probed by automated high-resolution filament tracking. *Biophys J* 93:346–359.
16. Gittes F, Mickey B, Nettleton J, Howard J (1993) Flexural rigidity of microtubules and actin-filaments measured from thermal fluctuations in shape. *J Cell Biol* 120:923–934.
17. Janson ME, Dogterom M (2004) A bending mode analysis for growing microtubules: Evidence for a velocity-dependent rigidity. *Biophys J* 87:2723–2736.
18. Ott A, Magnasco M, Simon A, Libchaber A (1993) Measurement of the persistence length of polymerized actin using fluorescence microscopy. *Phys Rev E* 48:R1642–R1645.
19. Tsyboulski DA, Bachilo SM, Weisman RB (2005) Versatile visualization of individual single-walled carbon nanotubes with near-infrared fluorescence microscopy. *Nano Lett* 5:975–979.
20. Tsyboulski DA, Rocha JDR, Bachilo SM, Cognet L, Weisman RB (2007) Structure-dependent fluorescence efficiencies of individual single-walled carbon nanotubes. *Nano Lett* 7:3080–3085.
21. Bachilo SM, et al. (2002) Structure-assigned optical spectra of single-walled carbon nanotubes. *Science* 298:2361–2366.
22. Aragon SR, Pecora R (1985) Dynamics of wormlike chains. *Macromolecules* 18:1868–1875.
23. Odijk T (1977) Polyelectrolytes near the rod limit. *J Polymer Sci B* 15:477–483.
24. Skolnick J, Fixman M (1977) Electrostatic persistence length of a wormlike polyelectrolyte. *Macromolecules* 10:944–948.
25. Gittes F, MacKintosh FC (1998) Dynamic shear modulus of a semiflexible polymer network. *Phys Rev E* 58:R1241–R1244.
26. Morse DC (1998) Viscoelasticity of tightly entangled solutions of semiflexible polymers. *Phys Rev E* 58:R1237–R1240.
27. Pasquali M, Shankar V, Morse DC (2001) Viscoelasticity of dilute solutions of semiflexible polymers. *Phys Rev E* 64:020802.
28. Shankar V, Pasquali M, Morse DC (2002) Theory of linear viscoelasticity of semiflexible rods in dilute solution. *J Rheol* 46:1111–1154.
29. Claessens MMAE, Bathe M, Frey E, Bausch AR (2006) Actin-binding proteins sensitively mediate F-actin bundle stiffness. *Nat Mater* 5:748–753.
30. Behabtu N, Green MJ, Pasquali M (2008) Carbon nanotube-based neat fibers. *Nano Today* 3:24–34.
31. Motta M, Moisala A, Kinloch IA, Windle AH (2007) High performance fibres from 'dog bone' carbon nanotubes. *Adv Mater* 19:3721–3726.

32. Elliott JA, Sandler JKW, Windle AH, Young RJ, Shaffer MSP (2004) Collapse of single-wall carbon nanotubes is diameter dependent. *Phys Rev Lett* 92:095501.
33. Kim UJ, Gutierrez HR, Kim JP, Eklund PC (2005) Effect of the tube diameter distribution on the high-temperature structural modification of bundled single-walled carbon nanotubes. *J Phys Chem B* 109:23358–23365.
34. Tsyboulski DA, Bachilo SM, Kolomeisky AB, Weisman RB (2008) Translational and rotational dynamics of individual single-walled carbon nanotubes in aqueous suspension. *ACS Nano* 2:1770–1776
35. Rai PK, et al. (2007) Dispersions of functionalized single-walled carbon nanotubes in strong acids: Solubility and rheology. *J Nanosci Nanotechnol* 7:3378–3385.
36. Arnold MS, Stupp SI, Hersam MC (2005) Enrichment of single-walled carbon nanotubes by diameter in density gradients. *Nano Lett* 5:713–718.
37. Odijk T (1983) On the statistics and dynamics of confined or entangled stiff polymers. *Macromolecules* 16:1340–1344.
38. Li GL, Tang JX (2004) Diffusion of actin filaments within a thin layer between two walls. *Phys Rev E* 69:061921.